Superdiffusion in dispersions of active colloids driven by an external field and their sedimentation equilibrium

Yen-Fu Chen,[1] Hsien-Hung Wei,[2] Yu-Jane Sheng,[1,*] and Heng-Kwong Tsao[3,4,†]

[1]*Department of Chemical Engineering, National Taiwan University, Taipei, Taiwan 106, Republic of China*

[2]*Department of Chemical Engineering, National Cheng Kung University, Tainan, Taiwan 701, Republic of China*

[3]*Department of Physics, National Central University, Jhongli, Taiwan 320, Republic of China*

[4]*Department of Chemical and Materials Engineering, National Central University, Jhongli, Taiwan 320, Republic of China*

The diffusive behaviors of active colloids with run-and-tumble movement are explored by dissipative particle dynamics simulations for self-propelled particles (force dipole) and external field-driven particles (point force). The self-diffusion of tracers (solvent) is investigated as well. The influences of the active force, run time, and concentration associated with active particles are studied. For the system of self-propelled particles, the normal diffusion is observed for both active particles and tracers. The diffusivity of the former is significantly greater than that of the latter. For the system of field-driven particles, the superdiffusion is seen for both active particles and tracers. In contrast, it is found that the anomalous diffusion exponent of the former is slightly less than that of the latter. The anomalous diffusion is caused by the many-body, long-range hydrodynamic interactions. In spite of the superdiffusion, the sedimentation equilibrium of field-driven particles can be acquired and the density profile is still exponentially decayed. The sedimentation length of field-driven particles is always greater than that of self-propelled particles.

I. INTRODUCTION

Microswimmers, such as omnipresent microbes in nature, can propel themselves to display active motion, and they adopt a wide range of swimming mechanisms. For example, *E. coli* bacteria whirl their flagella but ciliates beat their cilia for locomotion. Even though various differences exist among these mechanisms, all microswimmers live in the world of low Reynolds numbers [1] so that general features associated with their hydrodynamic behaviors are anticipated to be found. Brownian motion is usually neglected for microswimmers. However, it influences the behavior of nanoswimmers significantly [2,3]. Different from passive Brownian colloids which are at thermal equilibrium with their environment and move randomly, nanoswimmers viewed as active Brownian colloids are able to take up energy and convert it into directed motion. This process drives active colloids out of equilibrium. The nanopropulsion system has been a branch of nanotechnology and therefore it promises a variety of applications such as targeted delivery of cargo [4–7]. In addition, it is used to explore some core concerns of nonequilibrium statistical physics and has been investigated by theory [8–17], experiment [1–3,18–23], and simulation [24–41].

The run-and-tumble model is widely employed to describe the motions of active colloids. That is, active colloids would generally follow a series of approximately linear motions ("run"), which are intervened by sudden changes in their swimming direction ("tumble"). In general, the straight runs are characterized by a constant speed v_a and the tumbles come about randomly with a mean duration τ [8,9]. Dependent on the propulsion mechanism, two kinds of active colloids are considered in this study, self-propelled and field-driven

motion. For a self-propelled particle, the driving force exerted by the active colloid itself on the fluid is internally generated in the system through the flagella of bacteria [42,43] or chemical reactions catalyzed by Janus colloids [2,3,19]. The flow field generated around a self-propelled particle is similar to that by a force dipole. For a field-driven particle, the driving force is provided by the external field such as an optical trap [44] or a magnetic field [45–48]. Recently, it is reported that the turbulent state of the Janus particles, which consist of two hemispheres with different dielectric constants, can be driven by an ac electric field. Due to rotational Brownian motion and hydrodynamic interactions of the particles, their trajectories are not straight but random [49]. This experimental result reveals the run-and-tumble behavior of field-driven particles. However, different from self-propelled particles, the flow fluid created around a field-driven particle is similar to that by a force.

For the run-and-tumble organisms, their behaviors at large length and time scales are diffusive and can be depicted by Fick's law, where the diffusivity follows $D = v_a^2 \tau / d$ and d is the dimensionality [8,28]. The active motion of those microswimmers is not influenced by passive Brownian motion. As the diffusive trajectories of nanoswimmers are considered, however, the purely Brownian diffusivity (D_0) plays an important role in the effective diffusivity (D) driven partly by active motion. According to the experiment of artificial nanoswimmers, i.e., Janus active spheres in an H_2O_2 solution, the effective diffusivity obeys the relation $(D - D_0) \sim v_a^2 \tau_r$ based on the mean-squared displacement (MSD) analysis [2,19]. Here τ_r is the rotational diffusion time associated with the self-propelled colloid [10,27]. In addition to active colloids themselves, the motion of tracers (passive colloids or solvent) in a dispersion of active colloids has been studied as well. A hydrodynamic diffusion theory based on a Fickian constitutive law is employed to describe the diffusive behavior of a Brownian tracer particle in a dispersion of run-and-tumble

*yjsheng@ntu.edu.tw

†hktsao@cc.ncu.edu.tw

bacteria. When the Peclet number (Pe) is small, the hydrodynamic diffusivity of a tracer is proportional to $v_a^2(\tau/D_0)^{1/2}n$, where n is the number density of active colloids. In contrast, for large enough Pe and τ, the hydrodynamic diffusivity becomes independent of τ and is proportional to $v_a n$ [50].

An anomalous diffusive behavior is observed for the Brownian particle in a complex fluid or a biological system. Numerous examples include cytoskeleton dynamics [51], amoeboid locomotion [52], and cell migration [53]. The normal diffusive behavior is characterized by the linear growth of the mean-squared displacement (MSD) with time. However, for anomalous diffusion, the MSD $\langle \Delta r^2(t) \rangle$, in the three-dimensional case, deviates from the linear relationship and adopts the asymptotic form,

$$\langle \Delta r^2(t) \rangle = 6D_\alpha t^\alpha, \tag{1}$$

where D_α and α represent the generalized diffusion coefficient and the anomalous diffusion exponent, respectively. While the normal diffusion corresponds to $\alpha = 1$, the process is called the superdiffusion as $\alpha > 1$. A superdiffusive behavior is often observed in nonequilibrium systems driven by external active mechanisms [54–56]. Recently, it is reported that the superdiffusion of a particle immersed in a thermal reservoir is induced by a long-correlated external random force. That is, the particle disperses faster than the normal diffusion. Moreover, as the stochastic force is more correlated, the superdiffusive system approaches the ballistic limit ($\alpha \rightarrow 2$) [57]. In this work, the diffusive behaviors of the two types of active colloids driven by different propulsion mechanisms are explored by dissipative particle dynamics (DPD) simulations. The superdiffusive behavior is observed for run-and-tumble, field-driven particles because the hydrodynamic interactions among them are strong.

It is well known that the dispersion of passive colloids under gravity exhibits sedimentation equilibrium. The sedimentation of colloids is balanced by the Brownian diffusion which influences the sedimentation length (δ) in the barometric law. That is, the density of colloids at height z is depicted by $C(z)/C_0 = e^{-z/\delta}$. Because of the local fluid flow generated by active colloids and their diffusive behavior, it is anticipated that the sedimentation lengths of active colloids are different from those of passive colloids. Recently, nonequilibrium stationary states of active colloids have been studied both theoretically [8,9,12] and experimentally [3,19]. Evidently, those active particles behave as self-propelled particles. The experiment associated with field-driven particles is somewhat difficult to perform but the different behavior between self-propelled and field-driven particles should be clarified. In this study, the influences of those two types of active colloids on the sedimentation equilibrium are investigated by DPD as well.

II. MODEL AND SIMULATION METHOD

DPD, a particle-based mesoscopic simulation technique [58–60], can simulate the rheological and dynamic properties of fluids. Every DPD bead represents a cluster of atoms or molecules moving together, and their motions obey Newton's second law. The solvent particle (S) is represented by a DPD bead and the number density (ρ) is 3 generally. For simplicity,

an active particle (A) is also expressed by a single DPD bead in this work. The pairwise interactions between DPD beads contain the conservative force, dissipative force, and random force. These forces are purely soft-repulsive and apply to all beads within a cutoff radius ($r_c = 1$) beyond which the forces vanish. The detailed expression of those forces has been described elsewhere [39,61]. The conservative force between species i and j is characterized by the interaction parameter (a_{ij}), which is chosen as 25 for the same species ($a_{SS} = a_{AA} = 25$). To avoid effects other than hydrodynamics, $a_{AS} = 25$ is simply set for the interaction between active particles and solvent. The dissipative force between the fluid bead and the solid wall bead is six times greater than that between the fluid beads [62].

Two propulsion mechanisms of run-and-tumble active colloids are considered: force dipole and point force. The active force (F_a) is always imposed on an active colloid, and this force would change its direction randomly after a fixed period of time (τ). Note that the directions of all active forces are independent and they change their orientation asynchronously. For the case driven by force dipole, the particle is self-propelled in such a way that one solvent bead behind this particle is acted upon by an opposite force ($-F_a$). However, as the active force is originated from an external field, a point force exerts on the field-driven particle only and the reaction force does not exist, as illustrated in Fig. 1. More details have been disclosed elsewhere [38,41].

To examine the diffusive behaviors for both active colloids and solvent tracers, DPD simulations are implemented in a

Self-propelled active colloids (force dipole)

Field-driven active colloids (point force)
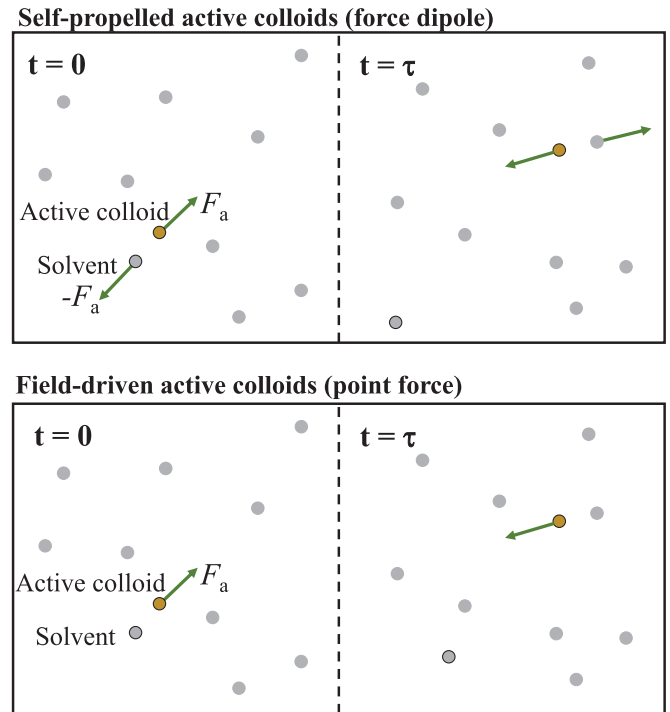
FIG. 1. Schematic diagram of the simulation systems: For the dispersion of self-propelled colloids, active colloids (yellow beads) and solvents (gray beads) are acted upon by F_a and $-F_a$, respectively. For the dispersion of field-driven colloids, only active colloids are acted upon by F_a. After each τ, the active force would change the direction randomly.

box ($30 \times 30 \times 30$) under periodic boundary conditions. For the sedimentation simulation, the upper and lower walls are constructed along the direction of the gravitational gradient (z axis) and the box size is $20 \times 20 \times 150$. The DPD time step is $\Delta t = 0.04$ to avoid the divergence of simulation and the total DPD steps are at least 10^6. The length, force, and time are scaled by the cutoff radius r_c and $k_B T / r_c$, and $(m r_c^2 / k_B T)^{1/2}$, respectively. Here $k_B T$ denotes the thermal energy and m is the mass of a DPD bead. For a bead with r_c about 1–10 nm at room temperature, the magnitude of the active force on nanoswimmers is about $O(1)$ pN.

III. RESULTS AND DISCUSSION

A. Effective diffusivity of fluid particles enhanced by self-propelled colloids

For both solvent bead and self-propelled colloid (driven by force dipole), their diffusivities can be obtained from either mean-squared displacement (MSD) or velocity autocorrelation function (VACF). The relationship between the diffusivity and MSD or VACF are given by

$$\langle \Delta r^2(t) \rangle = 6Dt, \tag{2}$$

$$D = \frac{1}{3} \lim_{t \to \infty} \int_0^t \langle \mathbf{v}(\tau) \cdot \mathbf{v}(0) \rangle d\tau, \tag{3}$$

where $\langle \mathbf{v}(t) \cdot \mathbf{v}(0) \rangle$ represents VACF of the target particle's velocity. Note that the above expressions are valid only as $t \gg \tau$. As the diffusivity of a self-propelled colloid has been previously studied and well understood [38], here we restrict our attention to the behavior of solvent particles. Our simulations reveal that the solvent particles are purely diffusive. We also confirm that the diffusivities evaluated from the two approaches agree with each other. Figure 2
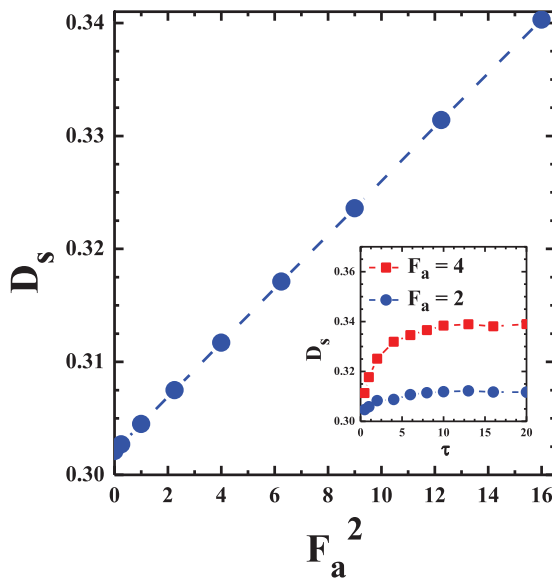
shows that the solvent diffusivity (D_s) grows quadratically with active force F_a at given run time τ and concentration of active particles ($\phi_p = 0.05$). In other words, with respect to the intrinsic diffusivity of solvent particle D_0, the solvent diffusivity is increased according to $(D_s - D_0) \propto F_a^2$, just like the active particle diffusivity. However, at a given F_a, D_s grows with τ at smaller τ until reaching a plateau at larger τ (see the inset), which is distinct from the diffusivity of active particle D_p that is proportional to τ [38]. The reason for the increase in D_s in the small τ regime is that the solvent particles around an active particle undergo frequent random kicking by the latter. Obviously, these solvent particles cannot move faster than the active particle since each of these particles merely receives part of the energy from the latter. But if τ is too large, these solvent particles will be less correlated except for those in the direction of F_a. Just like the case where a single particle is moving steadily in a bath of solvent particles, D_s cannot be increased indefinitely. Thus, for a sufficiently large τ, D_s has to stop growing with τ unless one increases F_a to have more solvent particles influenced by kicking from an active particle. This explains why the larger F_a is, the longer the τ needed for reaching the plateau. Because both $(D_s - D_0)$ and $(D_p - D_0)$ scale as F_a^2 with the former being saturated at large τ and the latter admitting a linear growth with τ [38], we conclude that D_s is always smaller than D_p; i.e., $D_s(F_a, \tau) < D_p(F_a, \tau)$.

The above results are made specifically for a sufficiently dilute suspension of active particles in which the active diffusivity depends mainly on active force F_a and run time τ. However, as the concentration of active particles ϕ_p is increased, the diffusivities of both active colloids and solvent particles are anticipated to be altered by substantial hydrodynamic interactions between active colloids. As shown in Fig. 3, the increment of D_s not only scales as v_a^2, but also grows linearly with ϕ_p. This increment is basically attributed to the fluid motion generated by active colloids as well as their collective hydrodynamic interactions. Since $(D_s - D_0)$ scales as v_a^2 for large enough τ (see Fig. 2),

FIG. 2. The variation of the diffusivity of solvents (tracers) in the dispersion of active self-propelled colloids with F_a^2 at $\tau = 16$ and $\phi_p = 0.05$. The variation of the solvent diffusivity with τ is in the inset.
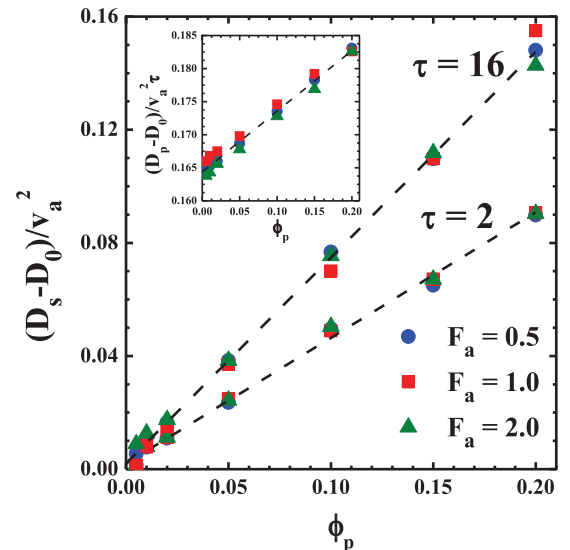
FIG. 3. The variations of $(D_s - D_0)/v_a^2$ and $(D_p - D_0)/v_a^2 \tau$ (inset) with ϕ_p.

its dependence on ϕ_p is universal, independent of F_a. The slope of the linear line $(D_s - D_0)/v_a^2$ vs ϕ_p for $\tau = 16$ is 0.73 and that for $\tau = 2$ is 0.45, giving $D_s = D_0 + 0.73\phi_p v_a^2$ and $D_s = D_0 + 0.45\phi_p v_a^2$, respectively. In contrast, for the active particle diffusivity, plotting $(D_p - D_0)/v_a^2\tau$ against ϕ_p collapses all the data points with various values of F_a and τ into a single straight line with the unique slope 0.092, as shown in the inset. Thus the active particle diffusivity can be expressed as $D_p = D_0 + (0.164 + 0.092\phi_p)v_a^2\tau$, which also agrees with the result in the dilute limit ($\phi_p = 0$) [38]. Unlike the diffusivity of self-propelled particles rising linearly with τ, the solvent diffusivity D_s does not grow linearly (see the inset of Fig. 2). As a result, the curves of the solvent diffusivity cannot collapse on a single line for a different run time.

B. Superdiffusion of field-driven colloids and fluid particles

If the motion of the active colloid is driven by an external field which changes the direction randomly after a time period of τ, the fluid flow around this active colloid is similar to that associated with a point force at low Reynolds number. The MSD and VACF of such field-driven colloids are evaluated and the trajectories of fluid particles (tracers) are monitored as well. At fixed F_a and τ the typical behaviors of MSD with various values of ϕ_p for both active colloids and fluid particles are shown in Figs. 4(a) and 4(b), respectively. Clearly, the results do not obey normal diffusion that displays a linear growth $\langle \Delta r^2(t) \rangle$ with respect to t. As seen from the log-log plot in the inset, the linear line with a slope $\alpha > 1$ is shown, indicating that $\langle \Delta r^2(t) \rangle$ grows like t^α. One might expect that the system goes back to normal diffusion at sufficiently long times. As illustrated in Fig. 4(c), the MSD of field-driven particles remains to evolve like t^α for a much longer time, although the linear behavior of MSD of self-propelled particles is readily seen at a very short time. Hence, the diffusive motion in this case is faster than normal diffusion.

In fact, both field-driven particles and tracers exhibit superdiffusive behavior with $\alpha > 1$. The abnormal diffusive behavior can be clearly demonstrated by VACF, as shown in Fig. 5(a). Compared to self-propelled particles [38], a very long tail in VACF of field-driven particles is observed. As a result, the integral of VACF in Eq. (3) grows with the upper limit of integration. Therefore, it is divergent as $t \to \infty$. Note that the velocity distributions for active colloids are deviated from the Maxwell-Boltzmann distribution because of F_a and are essentially similar to those reported in Ref. [38]. In addition to the direct analysis of MSD, the anomalous diffusion exponent (α) can also be determined from the analysis of VACF by [63]

$$\langle \Delta r^2(t) \rangle = 2t \int_0^t \left(1 - \frac{\tau}{t}\right) \langle \mathbf{v}(\tau) \cdot \mathbf{v}(0) \rangle d\tau = 6D_\alpha t^\alpha. \quad (4)$$

In the inset of Fig. 5(b), the exponents obtained from both MSD and VACF are compared to each other. The agreement between both approaches is clearly shown, verifying the superdiffusive behavior for field-driven particles and tracers.

Such superdiffusive behavior is essentially a result of strong hydrodynamic interactions between point force active particles, as the anomalous diffusion exponent (α) is found to be an increasing function of the concentration of active
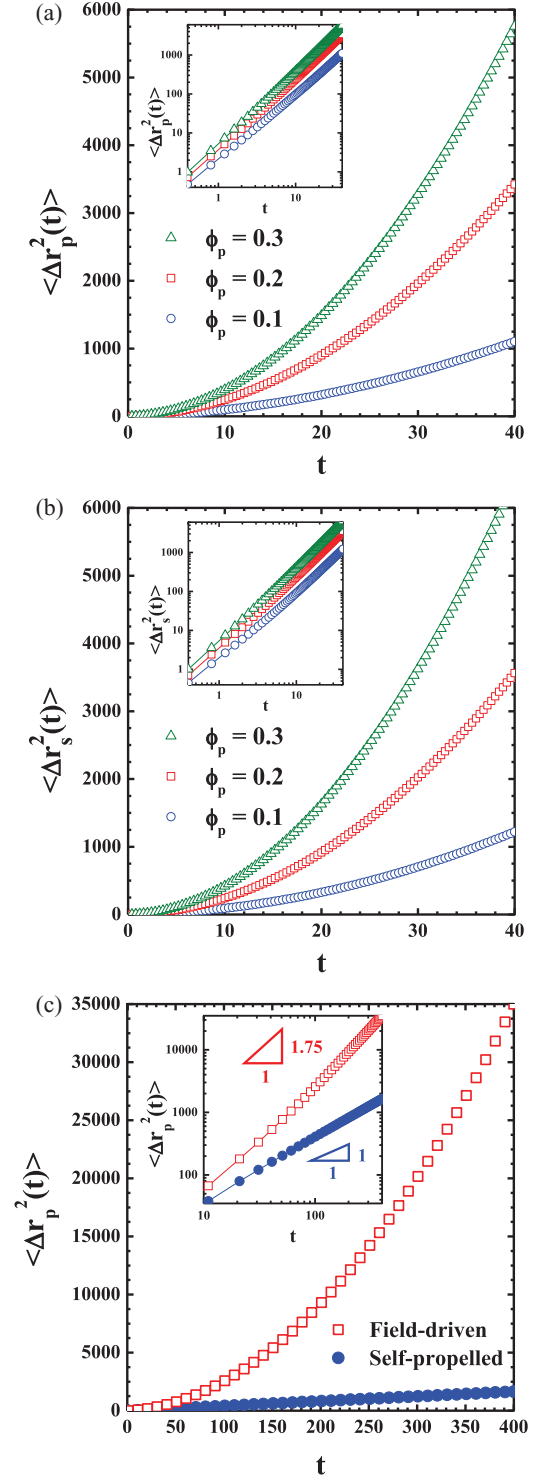
FIG. 4. (a) The variation of mean-squared displacement with t at $F_a = 2$ and $\tau = 16$ for field-driven colloids. The log-log representation is shown in the inset to demonstrate the power law behavior. (b) The variation of mean-squared displacement with t at $F_a = 2$ and $\tau = 16$ for solvent (tracers). The log-log representation is shown in the inset to demonstrate the power law behavior. (c) The variation of mean-squared displacement with t at $\phi_p = 0.03$, $F_a = 2.5$, and $\tau = 16$ for self-propelled colloids and field-driven colloids for $t = 0 - 400$. The slope in the inset represents the anomalous diffusion exponent α: 1 (normal diffusion) and 1.75 (superdiffusion).
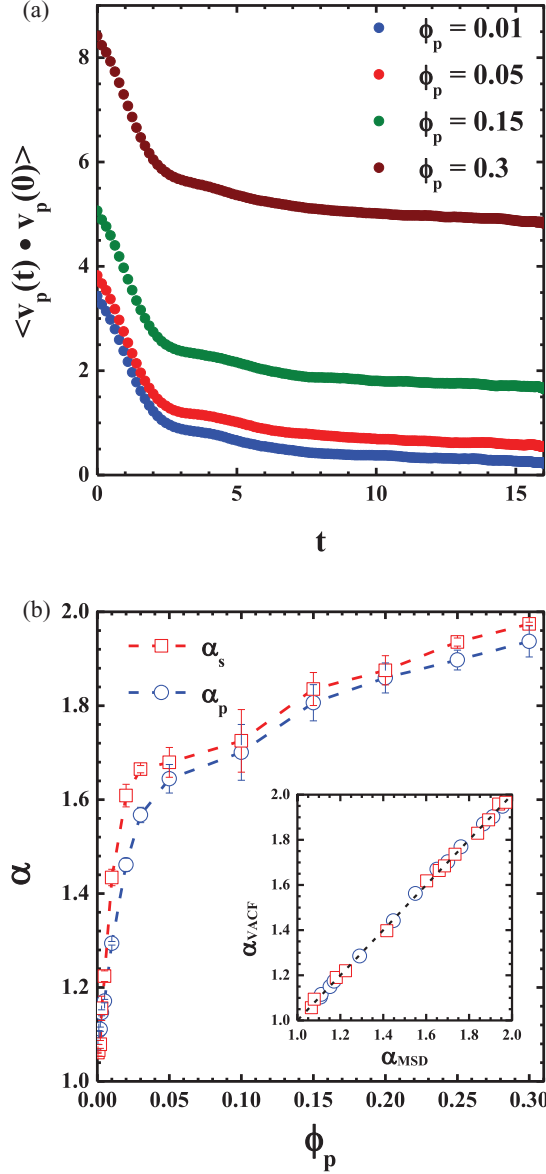
FIG. 5. (a) The velocity autocorrelation function of field-driven colloids $F_a = 2$ and $\tau = 16$ for different ϕ_p. (b) The variation of the anomalous exponent (α) with ϕ_p at $F_a = 2$ and $\tau = 16$ for the field-driven particles and solvents. The inset demonstrates the consistency between the results acquired from MSD and VACF.

FIG. 6. The variation of the anomalous exponent (α) with F_a at $\phi_p = 0.03$ and $\tau = 16$. The variation of α with τ at $\phi_p = 0.03$ and $F_a = 2$ is shown in the inset.

particles (ϕ_p). As shown in Fig. 5(b), α grows rapidly with ϕ_p in the small ϕ_p regime. But when ϕ_p exceeds 0.3, α approaches the ballistic limit ($\alpha \to 2$). Such a nontrivial increase of α with respect to ϕ_p seems to be a reminiscent of the divergence of the velocity variance when coming to evaluate VACF by accounting for pairwise hydrodynamic interactions between point force particles. (In contrast, for a suspension of self-propelled particles its velocity variance—because of the very rapid decay for point dipole interactions—is finite, rendering the effective particle diffusivity to be constant.) As will be shown later in Figs. 6 and 7, α also varies with F_a (or v_a) and τ. In the small ϕ_p regime, α would vary as a function of $v_a \tau / \ell$ characterized by a certain length scale ℓ. Because ℓ has to depend on ϕ_p, the only possible choice
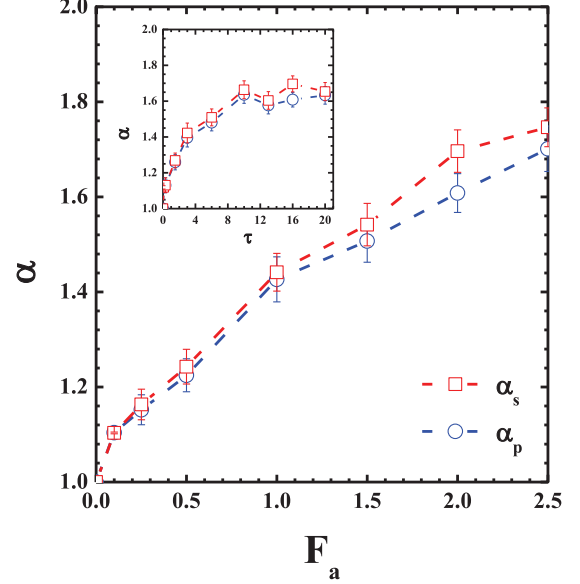
for ℓ is the mean particle separation $r_c \phi_p^{1/3}$, making α vary with $v_a \tau \phi_p^{1/3} / r_c$. Because Fig. 6 shows that $\alpha \propto v_a^n$ with $n < 1$, the above form suggests $\alpha \propto \phi_p^m$ with the exponent $m = n/3$ not greater than $1/3$, which explains the growing behavior of α in the small ϕ_p regime seen in Fig. 5(b). Such a particle-concentration-dependent diffusion exponent is quite unusual because it implies that the time correlation between any two consecutive movements for a test particle would actually depend on how the particle is correlated *spatially* to the surrounding particles. The latter is determined by hydrodynamic interactions. For point force active particles their hydrodynamic interactions would be so strong that a collective hydrodynamic force (through the spatial correlation) can be produced to alter the diffusive nature of each individual particle (through the time correlation).

When these active point force particles become very crowded, however, hydrodynamic interactions around a test particle would be limited to its nearby particles. While the particle movements might be slowed down by hydrodynamic interactions, these particles would undergo frequent collisions between each other. Because the collision time τ_{collide} in this case is much shorter than the run time τ, the particles are only correlated for time scale within τ_{collide}. The resulting VACF will look like a series of spikes separated by a constant time interval τ. Therefore, its time integration, which gives the diffusivity [see Eq. (2)], will be proportional to the number of collisions and hence time t. This explains why the particles can exhibit the ballistic behavior with $\alpha = 2$ when this special type of active suspension becomes sufficiently dense.

It is also interesting to observe that the anomalous diffusion exponent of solvent particles (α_s) is found to be always slightly larger than that of active particles (α_p) at specified F_a and τ; i.e., $\alpha_s(\phi_p) > \alpha_p(\phi_p)$. Hence for long times D_s will eventually outweigh D_p, which is different from $D_s < D_p$ for self-propelled particles. Hence, self-propelled and field-driven

particles have rather distinct diffusive behaviors. The distinction between these two different propulsion mechanisms manifests mostly in the way in which the diffusivity varies with the particle concentration. For self-propelled particles the diffusivity can grow linearly with the particle concentration, whereas for field-driven particles the anomalous diffusion exponent can rise more rapidly with the particle concentration in the dilute limit. Our results for superdiffusion may be relevant to intracellular transport of pigment organelles driven by myosin-V motors [56].

Aside from the concentration of active particles (ϕ_p), both the anomalous exponent (α) and generalized diffusion coefficient (D_α) can vary with F_a and τ as well. Figure 6 shows how α varies with F_a and τ at fixed $\phi_p = 0.03$. As F_a is increased, both α_s and α_p are increased because of strong hydrodynamic interactions. As τ is increased, both α_s and α_p rise first and then approach plateaus. In general, the anomalous exponent of the solvent is slightly greater than that of field-driven particles, $\alpha_s > \alpha_p$. This result associated with F_a or τ is consistent with that associated with ϕ_p. Figure 7 plots the variation of D_α with F_a and τ at $\phi_p = 0.03$. There exist minima for the generalized diffusion coefficients of field-driven particle ($D_{\alpha,p}$) and solvent ($D_{\alpha,s}$). Both $D_{\alpha,p}$ and $D_{\alpha,s}$ grow rapidly at large values of F_a but approach plateaus at large values of τ. Generally, one has $D_{\alpha,s} < D_{\alpha,p}$. Note that D_α approaches D_0 as $F_a \to 0$. The above results reveal that the superdiffusion of field-driven particles is mainly controlled by ϕ_p and F_a. For large enough τ, its saturation effect on D_α remains essentially the same as that in self-propelled particles. But unlike self-propelled particles, the diffusivity of the solvent (tracer) can be as strong as that of the active particle in a suspension of field-driven particles. The difference is mainly attributed to distinct hydrodynamic natures between self-propelled and field-driven particles: In the former hydrodynamic interactions between force dipoles

are weak, whereas those between point forces are strong in the latter.

C. Sedimentation equilibrium of field-driven colloids

It is well known that the sedimentation equilibrium of passive colloids subject to a constant force F_e along the z direction such as gravity can be depicted by the stationary solution of a drift-diffusion equation with the particle flux $J = -Ddc/dz + v_ec$, where v_e represents the terminal velocity associated with F_e. When the system reaches a steady state, the balance between upward diffusion and downward migration gives an exponential decay of the density profile $C(z)$ with a sedimentation length $\delta = D/v_e$. Recently, the sedimentation equilibrium of self-propelled colloids is also found to exhibit an exponential distribution with the sedimentation length that can also be determined from their effective diffusivity (D_p) [38]:

$$\delta = \frac{D_p(F_a, \tau)}{v_e(F_e)}. \qquad (5)$$

It is found that the effective diffusivity determined from MSD is consistent with that determined from δ in the sedimentation equilibrium, which varies with the active force and run time [38]. However, for active colloids driven by point forces, it is unclear how their sedimentation equilibrium is established because these particles are superdiffusive. Specifically, because the particle diffusivity here is not constant but growing with time, a stationary Boltzmann distribution cannot be obtained by simply setting the net particle flux to be zero in the drift-diffusion equation. Hence, Eq. (5) cannot be used to predict δ.

FIG. 7. The variation of the generalized diffusion coefficient (D_α) with F_a at $\phi_p = 0.03$ and $\tau = 16$. The variation of D_α with τ at $\phi_p = 0.03$ and $F_a = 2$ is shown in the inset.
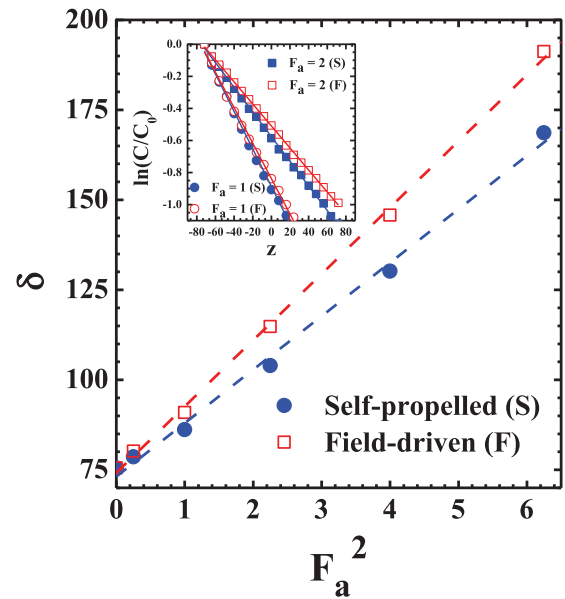
FIG. 8. The variation of the sedimentation length (δ) with F_a at $\phi_p = 0.03$ and $\tau = 16$ for self-propelled and field-driven colloids. The dimensionless density profile for different F_a is shown in the inset.
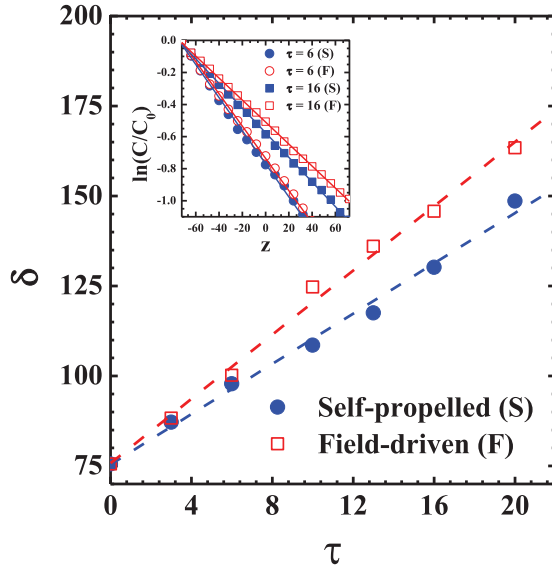
FIG. 9. The variation of the sedimentation length (δ) with τ at $\phi_p = 0.03$ and $F_a = 2$ for self-propelled and field-driven colloids. The dimensionless density profile for different τ is shown in the inset.

The DPD simulations of the sedimentation equilibrium for field-driven particles is performed subject to the downward force $F_e = 0.02$ at a fixed concentration of active particles ($\phi_p = 0.03$). For comparison, the simulation of the sedimentation equilibrium for self-propelled particles is carried out. The density profiles are obtained at various values of F_a and τ, as shown in the insets of Figs. 8 and 9. It is surprising to find that the density profiles for field-driven particles still obey the barometric law (exponential decay), similar to those for self-propelled particles. The sedimentation equilibrium is simply the consequence of the balance between downward flux by gravity and upward flux by random motion of active particles. Although active particles showing superdiffusion possess long-term memory in their velocities, they still have to obey the aforementioned balance and the particle density decreases with height. However, the density variation for field-driven particles extends over a greater length than that for self-propelled particles at the same F_a and τ. This is expected because field-driven particles are more diffusive than self-propelled particles.

By evaluating the sedimentation length δ for field-driven particles from the plot of $\ln C(z)$ against z, Figure 8 shows how δ varies with the active force F_a at $\tau = 16$. It is found that δ grows linearly with F_a^2, similar to that of self-propelled particles. Nonetheless, δ of field-driven particles is always greater than that of self-propelled particles at a given F_a. Figure 9 plots the variation of the sedimentation length with the run time τ at $F_a = 2$. Evidently, similar to self-propelled particles, δ of field-driven particles increases linearly with τ. Again, δ of the latter is always greater than that of the former at a given τ.

For self-propelled particles, δ is proportional to $F_a^2\tau$ because their effective diffusivity is $D_p \propto F_a^2\tau$ according to Eq. (5). Note that the diffusivity of the self-propelled

particle can be acquired from MSD, VACF, or δ [38]. All three approaches yield consistent results. For field-driven particles, however, their diffusive behavior is not normal but superdiffusive. Although the diffusive behaviors depicted by MSD and VACF are consistent, they are different from the approach of the sedimentation equilibrium. According to Eq. (5), it seems that the *apparent* diffusivity of field-driven particles can be defined from the sedimentation equilibrium and it is proportional to $F_a^2\tau$ as well. On the basis of the approach of δ, the apparent diffusivity of field-driven particles is always greater than that of self-propelled particles under the same values of F_a and τ owing to strong hydrodynamic interactions. Our analysis indicates that experiments like sedimentation equilibrium fail to distinguish particles with superdiffusion from those with normal diffusion but MSD and VACF are able to do so.

IV. CONCLUSIONS

In this work, we consider active particles with the run-and-tumble movement subject to active force F_a and run time τ. The diffusive behaviors of self-propelled particles (force dipole) and field-driven particles (point force) are explored by DPD simulations. The diffusion of solvent (tracer) is investigated as well. Both MSD and VACF approaches are employed and their results are consistent. For the system of self-propelled particles, the normal diffusion is observed for both active particles and solvent. The diffusivity of self-propelled particles is proportional to $\phi_p F_a^2\tau$, while the diffusivity of solvent is proportional to $\phi_p F_a^2$ for large enough τ. The former is significantly greater than the latter.

For the system of field-driven particles, the superdiffusion is seen for both active particles and solvents. Different from superdiffusive behavior in the literature, the mechanism of our superdiffusion is originated from strong hydrodynamic interactions. The anomalous exponent ($1 < \alpha < 2$) grows with increasing ϕ_p and F_a, while it approaches plateaus at large τ. It is surprising to find that in general, α of the solvent is slightly greater than that of active particles. That is, the MSD of the solvent is as significant as that of active particles, distinctly different from the system of self-propelled particles. This result is owing to the weak hydrodynamic interactions of self-propelled particles and the strong hydrodynamic interactions of field-driven particles. In spite of the superdiffusion, the sedimentation equilibrium of field-driven particles can be acquired and the density profile is still exponentially decayed. The sedimentation length of field-driven particles is always greater than that of self-propelled particles but is also proportional to F_a^2 and τ.

[1] S. Rafai, L. Jibuti, and P. Reyla, Phys. Rev. Lett. **104**, 098102 (2010).

[2] J. R. Howse, R. A. L. Jones, A. J. Ryan, T. Gough, R. Vafabakhsh, and R. Golestanian, Phys. Rev. Lett. **99**, 048102 (2007).

[3] G. Dunderdale, S. Ebbens, P. Fairclough, and J. Howse, Langmuir **28**, 10997 (2012).

[4] J. Burdick, R. Laocharoensuk, P. M. Wheat, J. D. Posner, and J. Wang, J. Am. Chem. Soc. **130**, 8164 (2008).

[5] S. Sundararajan, P. E. Lammert, A. W. Zudans, V. H. Crespi, and A. Sen, Nano Lett. **8**, 1271 (2008).

[6] S. Sundararajan, S. Sengupata, M. E. Ibele, and A. Sen, Small **6**, 1479 (2010).

[7] L. Baraban, M. Tasinkevych, M. N. Popescu, S. Sanchez, S. Dietrich, and O. G. Schmidt, Soft Matter **8**, 48 (2012).

[8] J. Tailleur and M. E. Cates, Europhys. Lett. **86**, 60002 (2009).

[9] J. Tailleur and M. E. Cates, Phys. Rev. Lett. **100**, 218103 (2008).

[10] R. Golestanian, Phys. Rev. Lett. **102**, 188305 (2009).

[11] B. ten Hagen, S. van Teeffelen, and H. Löwen, J. Phys.: Condens. Matter **23**, 194119 (2011).

[12] M. Enculescu and H. Stark, Phys. Rev. Lett. **107**, 058301 (2011).

[13] K. Martens, L. Angelani, R. Di Leonardo, and L. Bocquet, Eur. Phys. J. E: Soft Matter Biol. Phys. **35**, 84 (2012).

[14] A. Pototsky and H. Stark, Europhys. Lett. **98**, 50004 (2012).

[15] M. E. Cates and J. Tailleur, Europhys. Lett. **101**, 20010 (2013).

[16] K. Wolff, A. M. Hahn, and H. Stark, Eur. Phys. J. E: Soft Matter Biol. Phys. **36**, 43 (2013).

[17] Y. Fily, A. Baskaran, and M.C. Marchetti, Soft Matter **8**, 3002 (2012).

[18] X.-L. Wu and A. Libchaber, Phys. Rev. Lett. **84**, 3017 (2000).

[19] J. Palacci, C. Cottin-Bizonne, C. Ybert, and L. Bocquet, Phys. Rev. Lett. **105**, 088304 (2010).

[20] A. P. Berke, L. Turner, H. C. Berg, and E. Lauga, Phys. Rev. Lett. **101**, 038102 (2008).

[21] R. Di Leonardo, L. Angelani, D. Dell'Arciprete, G. Ruocco, V. Lebba, S. Schippa, M. P. Conte, F. Macarini, F. De Angelis, and E. Di Fabrizio, Proc. Natl. Acad. Sci. USA **107**, 9541 (2010).

[22] D. Yamamoto, A. Mukai, N. Okita, K. Yoshikawa, and A. Shioi, J. Chem. Phys. **139**, 034705 (2013).

[23] A. Guidobaldi, Y. Jeyaram, I. Berdakin, V. V. Moshchalkov, C. A. Condat, V. I. Marconi, L. Giojalas, and A. V. Silhanek, Phys. Rev. E **89**, 032720 (2014).

[24] P. T. Underhill, J. P. Hernandez-Ortiz, and M. D. Graham, Phys. Rev. Lett. **100**, 248101 (2008).

[25] J. P. Hernandez-Ortiz, P. T. Underhill, and M. D. Graham, J. Phys.: Condens. Matter **21**, 204107 (2009).

[26] Y.-G. Tao and R. Kapral, Soft Matter **6**, 756 (2010).

[27] I. O. Götze and G. Gompper, Phys. Rev. E **82**, 041921 (2010).

[28] R. W. Nash, R. Adhikari, J. Tailleur, and M. E. Cates, Phys. Rev. Lett. **104**, 258101 (2010).

[29] Y. Yang, V. Marceau, and G. Gompper, Phys. Rev. E **82**, 031904 (2010).

[30] D. Loi, S. Mossa, and L. F. Cugliandolo, Soft Matter **7**, 3726 (2011).

[31] F. Lugli, E. Brini, and F. Zerbetto, J. Phys. Chem. C **116**, 592 (2011).

[32] S. Thakur and R. Kapral, J. Chem. Phys. **135**, 024509 (2011).

[33] A. Kaiser, H. H. Wensink, and H. Löwen, Phys. Rev. Lett. **108**, 268307 (2012).

[34] J. Bialké, T. Speck, and H. Löwen, Phys. Rev. Lett. **108**, 168301 (2012).

[35] M.-B. Wan and Y. S. Jho, Soft Matter **9**, 3255 (2013).

[36] L. Zhu, E. Lauga, and L. Brandt, Phys. Fluids **24**, 051902 (2012).

[37] J. Elgeti and G. Gompper, Europhys. Lett. **101**, 48003 (2013).

[38] Z. Wang, H. Y. Chen, Y. J. Sheng, and H. K. Tsao, Soft Matter **10**, 3209 (2014).

[39] S. Xiao, Z. Wang, H. Y. Chen, Y. J. Sheng, and H. K. Tsao, J. Chem. Phys. **141**, 184902 (2014).

[40] J. Elgeti and G. Gompper, Europhys. Lett. **109**, 58003 (2015).

[41] Y. F. Chen, S. Xiao, H. Y. Chen, Y. J. Sheng, and H. K. Tsao, Nanoscale **7**, 16451 (2015).

[42] C. Brennen and H. Winer, Annu. Rev. Fluid Mech. **9**, 339 (1977).

[43] D. L. Koch and G. Subramanian, Annu. Rev. Fluid Mech. **43**, 637 (2011).

[44] M. E. J. Friese, T. A. Nieminen, N. R. Heckenberg, and H. Rubinsztein-Dunlop, Nature **394**, 348 (1998).

[45] B. A. Grzybowski, H. A. Stone, and G. M. Whitesides, Nature **405**, 1033 (2000).

[46] E. Climent, K. Yeo, M. R. Maxey, and G. E. Karniadakis, J. Fluids Eng. **129**, 379 (2007).

[47] A. Snezhko, M. Belkin, I. S. Aranson, and W.-K. Kwok, Phys. Rev. Lett. **102**, 118103 (2009).

[48] J. E. Martin and A. Snezhko, Rep. Prog. Phys. **76**, 126601 (2013).

[49] D. Nishiguchi and M. Sano, Phys. Rev. E **92**, 052309 (2015).

[50] T. V. Kasyap, D. L. Koch, and M. Wu, Phys. Fluids **26**, 081901 (2014).

[51] E. Zhou, X. Trepat, C. Park, G. Lenormand, M. Oliver, S. Mijailovich, C. Hardin, D. Weitz, J. Butler, and J. Fredberg, Proc. Natl. Acad. Sci. USA **106**, 10632 (2009).

[52] S. S. Rogers, T. A. Waigh, and J. R. Lu, Biophys. J. **94**, 3313 (2008).

[53] P. Dieterich, R. Klages, R. Preuss, and A. Schwab, Proc. Natl. Acad. Sci. USA **105**, 459 (2008).

[54] S. Khan, A. M. Reynolds, I. E. G. Morrison, and R. J. Cherry, Phys. Rev. E **71**, 041915 (2005).

[55] E. Hatta, J. Phys. Chem. B **112**, 8571 (2008).

[56] M. A. Despósito, C. Pallavicini, V. Levi, and L. Bruno, Physica A **390**, 1026 (2011).

[57] M. A. Despósito, Phys. Rev. E **84**, 061114 (2011).

[58] P. Español and P. Warren, Europhys. Lett. **30**, 191 (1995).

[59] R. D. Groot and P. B. Warren, J. Chem. Phys. **107**, 4423 (1997).

[60] K.-C. Huang, C.-M. Lin, H. K. Tsao, and Y. J. Sheng, J. Chem. Phys. **130**, 245101 (2009).

[61] A. Chaudhri and J. R. Lukes, Int. J. Numer. Methods Fluids **60**, 867 (2009).

[62] J. Xu, C. Yang, Y. J. Sheng, and H. K. Tsao, Soft Matter **11**, 6916 (2015).

[63] D. A. Mcquarrie, *Statistical Mechanics* (Harper and Row, New York, 1977).